Removal of phosphorus from aqueous solutions by granular mesoporous ceramic adsorbent based on Hangjin clay

Di Wang[a], Weiwu Hu[a,b,]*, Nan Chen[a,c], Yang Yu[a], Caixing Tian[a], Chuanping Feng[a,c]

[a]*School of Water Resources and Environment, China University of Geosciences (Beijing), Beijing 100083, China,*
Tel. +86 10 82322281; Fax: +86 10 82321081; email: hww2188@163.com (W. Hu)
[b]*The Journal Center, China University of Geosciences (Beijing), Beijing 100083, China*
[c]*Key Laboratory of Groundwater Cycle and Environment Evolution, China University of Geosciences (Beijing), Ministry of Education, Beijing 100083, China*

ABSTRACT

A new granular mesoporous ceramic adsorbent based on Hangjin clay was developed to evaluate the feasibility for phosphorus removal from aqueous environment. Batch experiments were performed to study the influence of various experimental parameters such as contact time, initial phosphorus concentration, initial pH, and surrounding temperature on the adsorption of phosphorus. Four kinetic models were tested, and the pseudo-second-order kinetic model fitted well with the adsorption kinetics. Besides that, the kinetic data were also fitted to the intra-particle diffusion model, presenting three linear regions, indicating that the kinetics of adsorption should follow multiple sorption rates. The equilibrium data revealed the Sips and Redlich–Peterson isotherm models fitted well with the phosphorus sorption process. The maximum adsorption capacity of ceramic adsorbent for phosphorus removal was 5.96 mg g^{-1}. The optimum phosphorus removal was observed between pH ranges of 4.0–12.0. The calculated thermodynamic parameters indicated that the adsorption process was spontaneous and endothermic in nature. Adsorption process appeared to be controlled by the mechanism of electrostatic attraction, ligand exchange, and chemical precipitation.

Keywords: Phosphorus removal; Hangjin clay; Redlich–Peterson model; Kinetics and isotherms; Adsorption mechanism

1. Introduction

Phosphorus has been known as an essential nutrient for the growth of organisms in ecosystem; however, amounts of soluble phosphorus in wastewater from household, agricultures, and industries could cause severe ecological problems such as algal blooms and eutrophication [1–3]. Additionally, limited availability of the exploitable reserves of phosphate rock emphasizes the need for phosphorus recovery from high P content wastewater [4]. On the basis of above considerations, it is essential to develop effective methods for removing phosphorus from effluents, while facilitating its recovery.

The conventional methods used to remove phosphorus from aqueous effluents include chemical precipitation [5], biological processes [6,7], ion exchange

[8,9], membrane technologies [10], and adsorption [11]. Among these methods, adsorption has been found to be superior to other techniques based on its high removal efficiency, easy operation, high efficiency, less sludge, and low cost [11]. A large number of adsorbents have been tested for the removal of phosphorus from aqueous solution, for example, hydrated metal oxide [12], Ca-based materials [13], and modified activated carbon [14,15]. Due to the high investment of these materials, a plenty of low-cost adsorbents such as agricultural waste, industrial tailings and different natural soil materials have gained significant research attention for phosphors removal in recent years. For example, Barca et al. reported high phosphorus adsorption capacity for steel slag [16], while Oguz found that the adsorption of phosphorus by blast furnace slag was effective [17]. Similarly, Karaca et al. analyzed effectiveness of dolomite in the removal of dissolved phosphate [18]. However, a major problem of using these adsorbents is the difficulty in separation after use since the adsorbents are present in powder form.

In China, rare earth mining produced a large amount of industrial tailings waste including the Hangjin clay every year. This clay is mainly present in Inner Mongolia of China and contains quartz, feldspar, calcite and amorphous iron oxide (Fe_2O_3). Many effective components of the Hangjin clay such as silicium, calcium, and aluminum and their oxides can be useful in the phosphorus removal [18]. In this work, a spherical particle was prepared from the Hangjin clay for the removal of phosphorus. The main objective of this study was to investigate the mechanism of phosphorus removal process at the solid–liquid interface based on the adsorption kinetic and isotherm characteristics. The study outcomes are expected to contribute to the recycling of rare earth tailings waste and phosphorus.

2. Materials and methods

2.1. Chemical reagents and adsorbent preparation

The Hangjin clay (particle size < 200 mesh) used in this study was obtained from the region of Hangjinqi (Ordos, China). Montmorillonite was purchased from the Zhenyongwei Technology Development Co., Ltd (Beijing, China). Corn straw was collected from the outskirts (Beijing, China), dried in an electric oven at $50 \pm 2°C$ for 48 h and milled with a small high-speed smashing machine (KINGSLH ZX-08, China) for 10 min before passing it through a 160 mesh sieve. Finally, the fine powders were stored at room temperature in an airtight container for further experiments.

All chemical reagents were of analytical grade, and were obtained from the Sinopharm Chemical Reagent Co., Ltd (Beijing, China). Phosphorus stock solution of 200 mg L^{-1} concentration was initially prepared by dissolving KH_2PO_4 reagent in deionized water and was serially diluted to obtain solutions at different concentrations for further experiments. The solution pH was adjusted with 0.1 M HCl and 0.1 M NaOH solutions.

The Hangjin clay, montmorillonite and corn straw powders were manually blended homogeneously at 2:1:1 (w/w/w) and mixed with deionized water. Montmorillonite was used as a bonding agent to enhance the stability of the adsorbent, while corn straw was used to increase the pore size. After the artificial granulation procedure, nearly spherical granular composite material with a diameter of 2–3 mm was prepared. The samples were then dried in an electric oven at $105 \pm 2°C$ for 24 h and calcined at $600°C$ for 1 h in a muffle furnace in the presence of air. Finally, the novel granular ceramic adsorbent was cooled to room temperature in a desiccator for further studies.

2.2. Batch studies

Batch studies were conducted in triplicates at room temperature ($25 \pm 2°C$) using 100-mL phosphorus solutions with initial concentrations of 10 and 50 mg L^{-1} in 250-mL conical flasks without any shaker in order to investigate the effect of contact time and adsorption kinetics. For the adsorption isotherm study, the initial phosphorus concentrations were varied between 5 and 100 mg L^{-1} at predetermined temperatures (10, 20, 30, and 40°C). The effect of pH was investigated by varying the pH in the range of 2.0–13.0, using 0.1 M HCl and 0.1 M NaOH solutions, at an initial phosphorus concentration of 10 mg L^{-1}. During the adsorption process, 1-mL aqueous sample was withdrawn at preset time intervals, and then filtered through a 0.45 μm cellulose acetate filter to determine the phosphorus concentration.

The amount of phosphorus adsorbed at any time per unit mass of the sorbent and the phosphorus removal efficiency were calculated using Eqs. (1) and (2) [15]:

$$q_t = \frac{(C_0 - C_e)V}{m} \tag{1}$$

$$R\,(\%) = \frac{(C_0 - C_e)}{C_0} \times 100\,\% \tag{2}$$

where q_t (mg g^{-1}) is the amount of phosphorus adsorbed per unit mass of sorbent at any time t (i.e. adsorption capacity); R (%) is the removal efficiency; C_0 (mg L^{-1}) and C_e (mg L^{-1}) are the initial and equilibrium phosphorus concentration in solutions, respectively; V (L) is the volume of phosphorus solution; and m (g) is the mass of sorbent added.

2.3. Analytical methods

Phosphorus analysis was carried out with a UV–visible spectrophotometer using the molybdenum antimony method at 700 nm (HACH-DR/5000, USA). A digital standard pH meter (ORION 8157BNUMD, USA) was used for pH measurement. Surface morphology of samples was analyzed using a scanning electron microscope (SEM) (SHIMADZU SSX-550, Japan). The specific surface area of samples was determined by the Brunauer–Emmett–Teller (BET) method with N$_2$ adsorption (COULTER ASAP2020 M, Japan). Elemental analysis of samples was undertaken using an electron probe microanalysis instrument (SHIMADZU EPMA1600, Japan). The crystalline structure of materials was characterized by the X-ray diffractometer (XRD) (D8 Focus, Germany). Fourier transform infrared (FTIR) spectroscopy (SHIMADZU IRPrestige-21, Japan) was used to investigate the presence of the functional groups in the samples before and after the experiments. The metal elements released were analyzed by the inductively coupled plasma optical emission spectrometer (ICP-OES) (THERMO ICAP6300, USA).

3. Results and discussion

3.1. Material characterization

The photos of original and treated samples are shown in Fig. 1(a) and (b), respectively. As evident from Fig. 1, a distinct thick layer of white crystals was attached on the surface of the treated sorbent in comparison to the original sorbent. The transformation of minerals during the adsorption is also evident in the SEM images. Fig. 1(c) and (d) show the surface characteristics of the original and treated sorbent at a magnification of 500×. It can be seen that Fig. 1(c) shows the samples had considerably loose and rough surface and complex drape trench texture morphology before phosphorus adsorption. But as seen from Fig. 1(d), the composite surface significantly changed with abundant agglomerates attached on the surface of the treated sorbent. Most of the rough drape structures were filled and covered by layered crystals, which can be attributed to the phosphorus adsorption onto the surface active sites. The typical nitrogen adsorption–desorption isotherms and their corresponding pore-size distributions (PSD) for the ceramic adsorbent are shown in Fig. 2(a). According to the International Union of Pure and Applied Chemistry (IUPAC) classification, the sample displayed the IV-type isotherm model, which is typical to many mesoporous adsorbents [19]. The hysteresis in the isotherm model appeared in the range of 0.44–0.98 of physisorption isotherms suggesting that capillary condensation took place in mesopores structures. In the range of relative pressure between 0.4 and 1.0, the shape of hysteresis loop resembles type-H3, which may be attributed to an increase in the N$_2$ sorption in mesoporous [19,20]. The corresponding pore size distribution of the original sample was determined using the Barrett–Joyner–Halenda (BJH) method from the adsorption isotherms. The PSD curve shows that the typical surface of the adsorbent is highly porous, with pore diameters ranging from 2 to 30 nm. Furthermore, the adsorbent had relatively high BET-specific surface area of 75.344 m^2 g^{-1}, and high total pore volume of 0.150 cm^3 g^{-1} (Table 1) that can facilitate the phosphorus adsorption.

The outcomes of the electron probe micro analysis (EPMA) of adsorbent are shown in Table 1. As evident
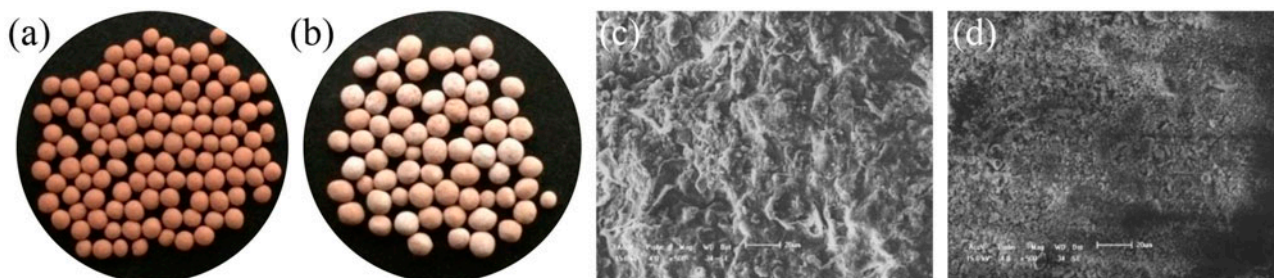
Fig. 1. Photo of (a) pristine granular ceramics and (b) granular ceramics after adsorption; SEM images of surface section of (c) pristine granular ceramics 500× and (d) granular ceramics after treated 500×.
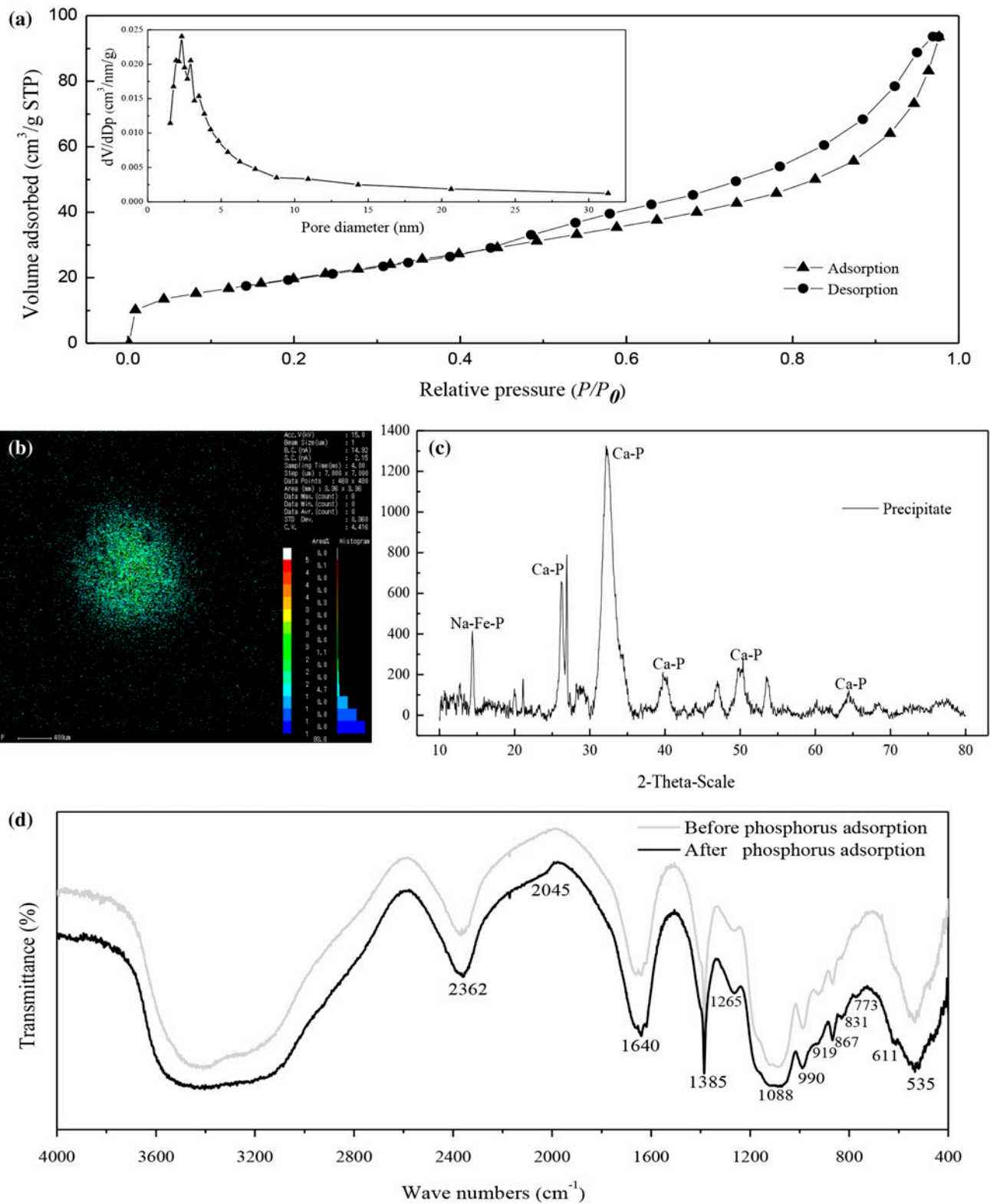
Fig. 2. (a) Nitrogen adsorption/desorption isotherms and pore size distribution curves of pristine granular ceramic adsorbent, (b) Mapping of P element analysis in treated adsorbent by Electron Probe Micro Analyzer (EPMA), (c) X-ray diffraction (XRD) of precipitate and (d) FTIR spectra of granular ceramics before and after adsorption phosphorus.

Table 1
Surface area characterization of pristine granular ceramics, component analysis of pristine/adsorbed granular ceramics, and solution precipitates

Surface area characterization (pristine)	S_{BET} (m² g⁻¹) 75.344			Pore volume (cm³ g⁻¹) 0.150			Average pore size (nm) 7.684		
Composition (wt%)	Ca	Si	Al	Fe	K	Mg	Na	O	P
Pristine sorbents	12.35	14.78	9.51	3.39	1.52	2.31	0.29	55.85	–
Treated sorbents	14.26	13.55	4.75	3.67	1.28	1.83	0.35	51.91	8.40
Solution precipitate	26.51	3.52	2.03	1.31	0.23	0.25	–	51.30	14.85

in Table 1, the original adsorbent contained abundant metal/nonmetal elements (M) and their oxide compounds (MO). The percentage mass content of Ca, Fe, and K ions shows no significant changes between original and treated adsorbent. However, decreased amount of Al, Si, and Mg ions was found in treated adsorbent, which could be due to the loss of some elements via hydration and dissolution. Phosphorus appeared on the surface of the treated adsorbent with a weight percentage of 8.40%, indicating that phosphorus was bound to the active sites present on the surface of adsorbent. The precipitates obtained after adsorption primarily contained P and Ca with the weight percentages of 14.85 and 26.51%, respectively, along with a small amount of elements such as Al, Fe, and Si (Table 1). P elemental analysis by EPMA mapping in Fig. 2(b) also shows that P was adsorbed well and dispersed throughout the entire surface of the adsorbent, indicating that the ceramic adsorbent had been effective for phosphorus removal. The X-ray diffraction pattern of precipitate powder is presented in Fig. 2(c). It was found clearly that the main component in precipitation was hydroxyapatite, which suggested that the uptake of phosphorus ions is partly by chemical adsorption.

The FTIR spectra of original and treated ceramic adsorbent are shown in Fig. 2(d). The figure displays a number of absorption peaks, indicating that the material had complex chemical characteristics. The infrared spectrum suggested adsorbent heterogeneity, which was further confirmed by different characteristic peak with the possible presence of hydroxyl (535, 611, 3,200–3,600 cm⁻¹), hydrocarbyl (2045, 2,360 cm⁻¹) and carbonyl (1,640 cm⁻¹) groups, C–H bending bond (867, 990 cm⁻¹) and C–O stretching bond (773, 831, 1,265 cm⁻¹) of carboxyl groups, CH₃ symmetrical deformation mode (1,385 cm⁻¹) and C–O–C bonds (1,088 cm⁻¹) [21]. Smoother and red shifted bands were observed in the spectrum after adsorption of phosphorus at about 3,200–3,600 cm⁻¹. This can be attributed to the complexation of phosphate ions with the ionized hydroxyl and to the bond with O–H bands of carboxylic acids leading to a weak O–H stretching vibration. The changes in functional groups and surface properties of adsorbent were illustrated by the stretching transformation of several key bands, and further indicate the existence of ligand exchange mechanism between phosphate and –OH on the sorbent surface during the sorption process.

3.2. Effect of contact time and adsorption kinetics

The effects of contact time and the phosphorus sorption kinetic characteristics were investigated to determine the phosphorus adsorption rate and the main sorption mechanisms. As evident from Fig. 3(a), the slope is relatively steep during the initial 10 h suggesting a rapid adsorption rate. This can be attributed to the significant amount of free surface area were available on the ceramic leading to the adsorption of a large number of phosphate ions onto the adsorbent. Since the availability of free surface areas decreases subsequently, the rate of phosphorus adsorption decreased [22]. Consequently, the removal rate gradually slows after 10 h. It is worthy to note that only insignificant amount of phosphorus removal takes place after 24 h. Thus, the optimum contact time for the adsorption was taken as 24 h.

Four kinetic models, including pseudo-first-order, pseudo-second-order, Elovich, and intra-particle diffusion models, were used to investigate the phosphorus adsorption kinetics. The first two models are based on the adsorption capacity, predicting the behavior over the concentration range investigated and assume that the physisorption and chemisorption are the rate-controlling steps. Two nonlinear kinetic equations are given below as Eqs. (3) and (4) [23], respectively:

$$q_t = q_e \left(1 - e^{(-k_1 t)}\right) \tag{3}$$
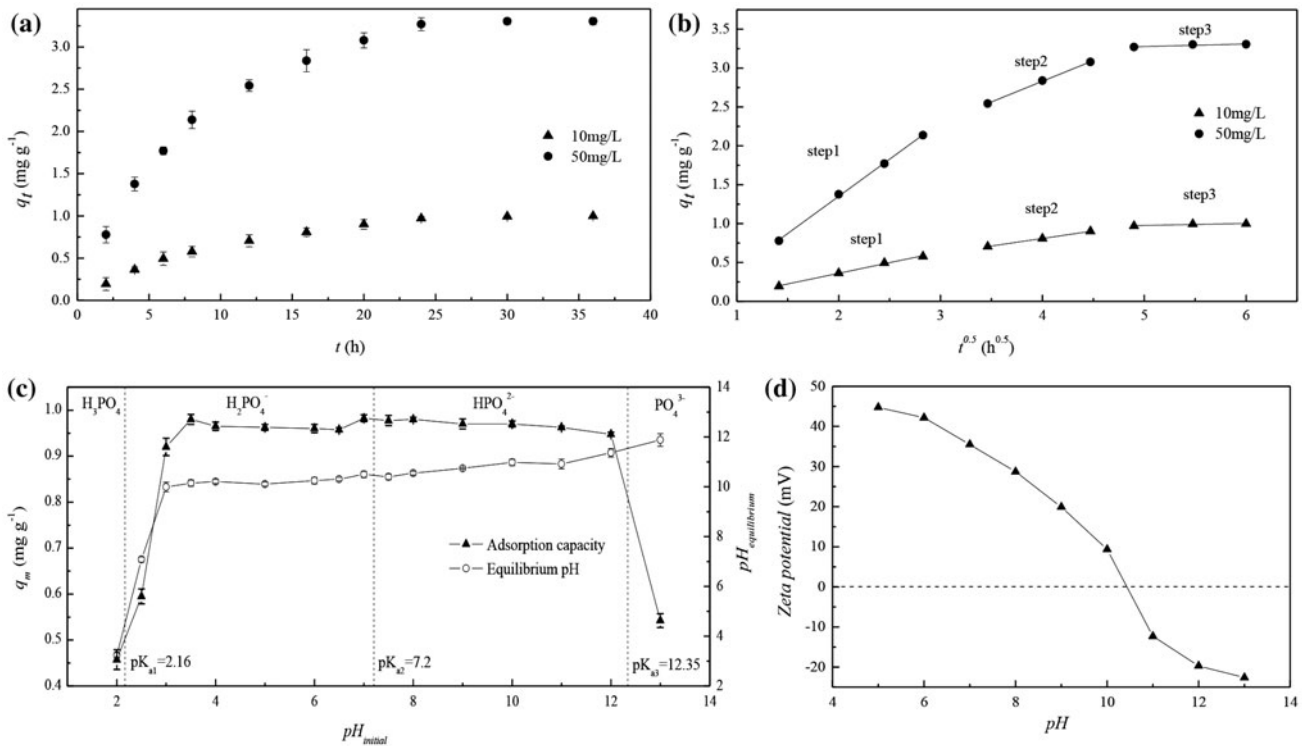
Fig. 3. (a) Effect of contact time, (b) Initial-particle diffusion modeling, (c) Effect of initial pH on phosphorus adsorption, and (d) Effect of pH on the zeta-potential of adsorbent. Initial phosphorus concentration 10 and 50 (mg L^{-1}), adsorbent dosage 1 (g 100 mL^{-1}), and temperature 25 ± 2℃.

$$q_t = \frac{k_2 \, q_e^2 \, t}{1 + k_2 \, q_e t} \quad (4)$$

where q_e and q_t are the amount of phosphorus adsorbed (mg g^{-1}) at equilibrium and at time t (h), respectively, k_1 (h^{-1}) and k_2 (g mg^{-1} h^{-1}) are the first- and second-order reaction rate constant, respectively. The χ^2 and R^2 values for the pseudo-second-order model were slightly batterer than that for the pseudo-first-order model (Table 2) suggesting that the phosphorus adsorption kinetics followed the pseudo-second-order model well. It can be indicated that the chemical adsorption is the process of rate-limiting step [24]. Similar results were also reported by previous researchers [25,26].

The Elovich equation is for general application to chemisorption kinetics [27]. This model has been applied satiafactorily to some chemisorption processes and has been found to cover a wide range of slow adsorption rates. The Elovich kinetic model could be written as [28]:

$$q_t = \left(\frac{1}{\beta}\right) \ln^{(\alpha \beta)} + \left(\frac{1}{\beta}\right) \ln^{(t)} \quad (5)$$

where α (mg g^{-1} h^{-1}) is the initial adsorption rate and β (g mg^{-1}) is related to the extent of surface coverage and the activation energy involved in chemisorption. It could be stressed that although the best R^2 value obtained with the concentrated solution of phosphorus (50 mg L^{-1}), conversely, with the lower initial concentration of phosphorus (10 mg L^{-1}), the value of R^2 was little bit worse.

The kinetic experimental data were further analyzed with the intra-particle diffusion model. The adsorption mechanism followed a three-stage process: film diffusion, intra-particle diffusion and ion binding on active sites. The linear form of the equation is given in Eq. (6) [29], which can confirm the presence or absence of intra-particle diffusion:

$$q_t = k_{id} \, t^{1/2} + C \quad (6)$$

where k_{id} (mg g^{-1} h$^{-1/2}$) is the intra-particle diffusion rate constant, while $i = 1$–3 represents the three stages of adsorption, respectively; and C is the constant indicating the thickness of the boundary layer. The intra-particle diffusion is the only rate-controlling step if the plot is linear and passes through the origin. The parameters k_{id} and C can be determined from the

Table 2
Kinetic models constants for sorption of phosphorus at different initial phosphate concentration. Initial phosphorus concentrations 10 and 50 (mg L^{-1}), adsorbent dosage 1 (g 100 mL^{-1}), and temperature 25 ± 2°C

	Initial concentration (mg L^{-1})	
	10	50
Pseudo-first-order		
k_1 (h^{-1})	0.1010	0.1231
q_e (mg g^{-1})	1.0408	3.3837
χ^2	0.0036	0.0032
R^2	0.9950	0.9956
Pseudo-second-order		
k_2 (g mg^{-1} h^{-1})	0.0627	0.0263
q_e (mg g^{-1})	1.3986	4.3789
χ^2	0.0015	0.0028
R^2	0.9972	0.9964
Elovich		
α (mg g^{-1} h^{-1})	0.2699	1.0895
β (g mg^{-1})	3.3224	0.9807
χ^2	0.0551	0.0018
R^2	0.9935	0.9979
Intra-particle diffusion		
k_{1d} (mg g^{-1} h$^{-0.5}$)	0.6737	0.9553
R_1^2	0.9952	0.9985
k_{2d} (mg g^{-1} h$^{-0.5}$)	0.1933	0.5310
R_2^2	0.9998	0.9989
k_{3d} (mg g^{-1} h$^{-0.5}$)	0.0256	0.0327
R_3^2	0.9022	0.8304

slope and the intercept of the linear plot of q_t vs. $t^{1/2}$, respectively, as shown in Fig. 3(b).

Fig. 3(b) clearly shows that the plot is not a straight line over the entire time range. Three steps are shown on the curve with the first line corresponds to the external surface adsorption while the second line represents the internal surface adsorption. The presence of the third line on the curve is attributed to the presence of the saturation step. In addition, k_{1d} was greater than k_{2d} and k_{3d} in Table 2, indicating that the external surface adsorption was significantly faster than the intra-particle diffusion. Furthermore, the curve did not pass through the origin ($C_i \neq 0$) suggesting that the intra-particle diffusion was not the only rate-limiting step [29]. Therefore, both film diffusion and pore diffusion were likely to have influenced the adsorption process.

3.3. Adsorption equilibrium isotherm

The adsorption isotherm describes the relationship between the amount of adsorbate uptaken by the adsorbent and the adsorbate concentration remaining in solution [28]. There are many equations for analyzing experimental adsorption equilibrium data. The equation parameters of these models often provide some insight into the adsorption mechanism. In this study, the Langmuir, Freundlich, Sips and Redlich–Peterson isotherm models were tested.

The Langmuir isotherm model assumes that the adsorbent surface is homogenous and the adsorption energy for each adsorption site is equivalent. Solute immobilization occurs without mutual interactions between the molecules adsorbed at the surface [30]. The nonlinear forms of the Langmuir isotherm equation is:

$$\frac{q_e}{C_e} = \frac{1}{K_L\,q_m} \tag{7}$$

where q_e (mg g^{-1}) is the amount of solute sorbed per unit weight of material; C_e (mg g^{-1}) is the equilibrium concentration of phosphorus; q_m (mg g^{-1}) is the maximum adsorption capacity of the material, and K_L (L mg^{-1}) are the Langmuir constants corresponding to the binding energy of the sorption system.

The Freundlich model is based on an exponential distribution of adsorption sites and energies, and mutual interaction between adsorbed molecules is possible [30]. The nonlinear forms of the Langmuir and Freundlich equations are expressed as [31]:

$$q_e = K_F\,C_e^{1/n} \tag{8}$$

where K_F (mg g^{-1}) and $1/n$ are the empirical constants in the Freundlich isotherm, indicating that the sorption capacity factor and intensity parameter, respectively.

The Sips model is empirical and it consists of the combination of the Langmuir and Freundlich isotherm type models. This model takes the following form [32]:

$$q_e = \frac{q_m\,K_S\,C_e^{1/n}}{1 + K_S\,C_e^{1/n}} \tag{9}$$

where K_S (mg L^{-1}) is the Sips constant related with affinity constant and $1/n$ is the Sips exponent.

The Redlich–Peterson model also is an empirical equation that describes an equilibrium isotherm [33]:

$$q_e = \frac{K_{RP} C_e}{1 + a_{RP} C_e^g} \qquad (10)$$

where K_{RP} (L mg^{-1}) and a_{RP} (mg L^{-1}) are Redlich–Peterson constants and g is the Redlich–Peterson dimensionless, whose value should be ≤1. This equation reduces to a linear isotherm in the case of low surface coverage ($g = 0$) and to a Langmuir isotherm when $g = 1$ [28].

The data of the fitted models are presented on Table 3. Based on the χ^2 and R^2 values, the Langmuir, Sips and Redlich–Peterson isotherm models show a better fit than the Freundlich model at low temperature (10 and 20°C). This indicates that phosphate ions were adsorbed in the form of monolayer coverage on the surface of adsorbent at low temperature. Conversely, the Freundlich, Sips, and Redlich–Peterson models show a better fit with the experimental data at higher temperatures such as 30 and 40°C. This implies

that a multilayer adsorption occurred in the process of phosphorus removal at a high temperature.

A comparative study to most other reported adsorbents was performed. The results are presented in Table 4, which suggested that the Hangjin clay granular ceramic adsorbent had a relative higher affinity toward phosphorus molecules among those sorbents. Therefore, Hangjin clay was suitable and promising for phosphorus removal from aqueous solutions since it has a relatively high adsorption capacity.

3.4. Adsorption thermodynamics

The adsorption thermodynamics characteristics were analyzed to investigate the adsorption process. The thermodynamic equilibrium constants (K_d) of the adsorption process were calculated as the ratio of the amount of adsorbate removed at equilibrium to the equilibrium solution concentration (q_e/C_e). ΔH and ΔS were calculated from the slope and intercept of ln K_d vs. $1/T$ plot using Eq. (11). The Gibbs free energy change (ΔG) for the adsorption on composite sorbent is related to ΔH and ΔS, which represent changes in enthalpy and entropy, respectively, as expressed in Eq. (12):

$$\ln K_d = \frac{\Delta S}{R} - \frac{\Delta H}{RT} \qquad (11)$$

$$\Delta G = \Delta H - T\Delta S \qquad (12)$$

where R and T are the gas constant (8.314 J mol^{-1} K^{-1}) and Kelvin temperature, respectively.

Table 3
Isotherm constants for phosphate adsorption at different temperatures. Initial phosphorus concentrations 10–100 (mg L^{-1}), adsorbent dosage 1 (g 100 mL^{-1}), and temperatures 10, 20, 30, and 40°C

	Temperature (°C)			
	10	20	30	40
Langmuir model				
q_{max} (mg g^{-1})	3.689	4.0306	5.359	5.8936
K_L (L mg^{-1})	0.2638	0.3146	0.276	1.4414
χ^2	0.0151	0.0295	0.6498	1.4288
R^2	0.9937	0.9902	0.886	0.8545
Freundlich model				
K_F (mg g^{-1})	0.9895	1.1338	1.5695	2.0720
$1/n$	0.3232	0.3199	0.3254	0.3530
χ^2	0.1416	0.1403	0.0492	0.3186
R^2	0.9412	0.9536	0.9913	0.9675
Sips				
q_{max} (mg g^{-1})	1.7468	3.1604	4.4762	5.9583
K_s (mg L^{-1})	0.2794	0.2949	0.0074	0.0046
n_s	1.2784	1.2608	3.0698	2.8302
χ^2	0.0182	0.0266	0.0542	0.0885
R^2	0.9961	0.9942	0.9932	0.9754
Redlich–Peterson				
K_{RP} (L mg^{-1})	1.2866	1.7261	3.9121	5.4784
a_{RP} (mg L^{-1})	0.4977	0.6588	1.9200	2.1200
g	0.9114	0.8969	0.6747	0.6472
χ^2	0.0075	0.0119	0.0438	0.0779
R^2	0.9983	0.9974	0.9924	0.9616

Table 4
Adsorption capacity of calys and some other adsorbents for phosphorus removal

Adsorbents	q_m (mg g^{-1})	Refs.
BOF-modified slags	2.49	[16]
Tablet porous material	4.39	[22]
Ground burnt patties	0.43	[24]
Hydrous niobium oxide	2.90	[25]
Natural palygorskite clay	10.9	[26]
Zeolite	0.71	[34]
ZrO$_2$-Fe$_3$O$_4$-modified carbon	4.51	[35]
La-modified Bentonite	8.59	[36]
Coir pith	4	[37]
Posidonia oceanica fibers	7	[38]
ZnCl$_2$-modified activated carbon	4.2	[39]
Al-pillared bentonite	5.05	[40]
Hangjin clay granular ceramic	5.89	This study

The ΔG, ΔH, and ΔS values for the adsorption of phosphorus onto ceramic adsorbent are listed in Table 5. The negative values for ΔG indicate that the adsorption process was spontaneous. The ΔS is positive, which shows that the increase in randomness during the phosphorus adsorption process. The positive ΔH value indicates that adsorption of phosphorus was endothermic in nature, further highlighting that high temperature is beneficial to the occurrence of adsorption reaction. It can be hypothesized from the enthalpy value that the adsorption forces on the sorbent surface were mainly the hydrogen and dipole bonds, along with the van der Waals force.

3.5. Effect of initial pH on phosphorus adsorption

The pH of aqueous solution is an important variable that influences the adsorption process of sorbates at the solid–liquid interface. According to Fig. 3(c), the phosphorus adsorption capacity increased when pH was below 3.0, and reached the peak at pH 3.5. The adsorption almost remained stable between 3.0 and 12.0, while the amount of phosphorus adsorption began to decrease after pH 12.0.

Phosphate exists in the form of H_3PO_4, $H_2PO_4^-$, HPO_4^{2-}, and PO_4^{3-} at different pH according to the acid dissociation constant values of phosphoric acid, as shown in Eq. (13) [41]:

$$H_3PO_4 \xoverset{pK_{a1}}{\longleftrightarrow} H^+ + H_2PO_4^- \xoverset{pK_{a2}}{\longleftrightarrow} 2H^+ + HPO_4^{2-} \xoverset{pK_{a3}}{\longleftrightarrow} 3H^+ + PO_4^{3-} \tag{13}$$
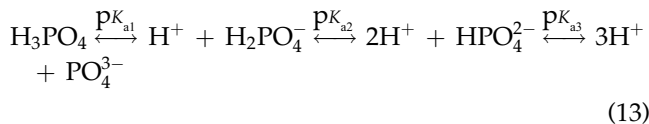
where $pK_{a1} = 2.16$, $pK_{a2} = 7.20$, $pK_{a3} = 12.35$, respectively.

Previous studies have noted that certain anions were adsorbed for ligand exchange via outer-sphere and inner-sphere complexation. The former involves electrostatic attraction and demands a water molecule retained between the exchange sites and the ligand [42], while the latter is formed by covalent bonding

between the metal ions and ligand [43]. Table 1 shows that granular ceramic contained significant amount of silicon oxide and other metal oxides. The ligand (–OH) can bond with these metal/nonmetal oxides (MO) hydrates to form $\equiv M–OH$ when the granular sorbent was impregnated in aqueous solutions, as shown in Eq. (14). The effect of pH on the zeta potential of original adsorbent is shown in Fig. 3(d), in which the isoelectric point pHzpc of adsorbent is at about the point 10.5. When the pH was varied from 3 to 10, the surface of adsorbent was protonated, as seen in Eq. (15). In this pH range, the dominant phosphate forms are monovalent $H_2PO_4^-$ ion and divalent HPO_4^{2-} ion. Protonated active sites can favor the electrostatic attraction to the phosphate species, and the outer-sphere complex formation can be described by following Eqs. (17)–(18) [42,43]:

$$MO + H_2O \longrightarrow \equiv M - OH \tag{14}$$

$$\equiv M - OH + H^+ \longrightarrow \equiv M - OH_2^+ \tag{15}$$

$$\equiv M - OH \leftrightarrow \equiv M - O^- + H^+ \tag{16}$$

$$\equiv M - OH_2^+ + H_2PO_4^- \leftrightarrow \equiv M - (OH_2^+)(H_2PO_4^-) \tag{17}$$

$$\equiv M - OH_2^+ + HPO_4^{2-} \leftrightarrow \equiv M - (OH_2^+)(HPO_4^{2-}) \tag{18}$$
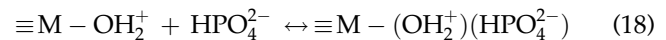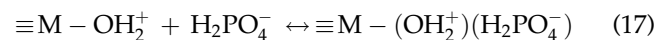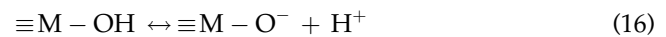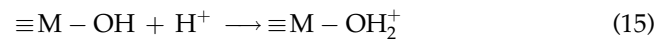
In addition, at acidic pH, H^+ ions in aqueous solutions can favor the inner-sphere ligand exchange, as seen in Eqs. (19)–(20). Considering the structure of ceramic adsorbent, the $H_2PO_4^-$ and HPO_4^{2-} can react with M–OH via hydrogen bonding according to Eqs. (21)–(22) [44]:

$$\equiv M - OH + H_2PO_4^- \leftrightarrow \equiv M - (H_2PO_4) + OH^- \tag{19}$$

$$2 \equiv M - OH + HPO_4^{2-} \leftrightarrow M_2 - (HPO_4) + 2OH^- \tag{20}$$
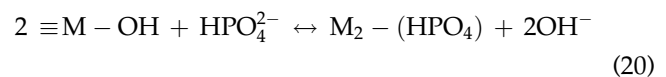
Table 5
Thermodynamic parameters for phosphate adsorption for phosphate adsorption at different temperature. Initial phosphorus concentrations 10–100 (mg L^{-1}), adsorbent dosage 1 (g 100 mL^{-1}), and temperatures 10, 20, 30, and 40°C

Temperature (°C)	ΔG (kJ mol^{-1})	ΔS (J mol^{-1} K^{-1})	ΔH (kJ mol^{-1})
10	−19.42	68.71	24.18
20	−20.11		
30	−20.79		
40	−21.48		

$$\equiv M - OH + H_2PO_4^- \leftrightarrow M - OH \ldots H_2PO_4^- \qquad (21)$$

$$\equiv M - OH + HPO_4^{2-} \leftrightarrow M - OH \ldots HPO_4^{2-} \qquad (22)$$
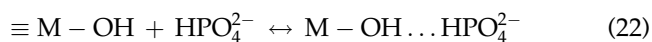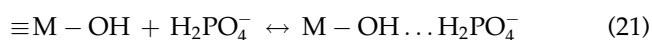
However, when the solution pH was increased and above the isoelectric point, the active sites were deprotonated (Eq. (16)), leading to more negative charges on adsorbent surface causing electrostatic repulsion between phosphate species and the negatively charged adsorbent surface. Additionally, the existence of a competition between phosphate and hydroxide groups can disturb the occurrence of ligand exchange. Nevertheless, there was only a slight decrease in the adsorption capacity at pH between 10.0 and 12.0. Several studies found that the rise of solution pH to alkaline can be favorable to the precipitation of calcium phosphate. Consequently, the ceramic sorbent can be still effective in the phosphorus removal at the pH range between 7.0 and 12.0 (Eq. (23)). In addition, a small quantity of Al, Fe, and Mg ions that were leached from adsorbent also can react with phosphate to form the following possible precipitates [44]:

$$5Ca^{2+} + 3HPO_4^{2-} + 4OH^- \longrightarrow Ca_5(PO_4)_3OH + 3H_2O \qquad (23)$$
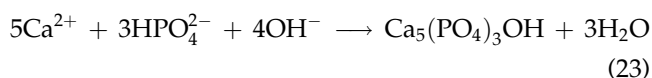
The decrease in phosphorus adsorption after pH 12.0 can be due to the formation of the dominant phosphate PO_4^{3-} ion, which has a tendency to form only a weak bond with the active sites of the sorbent. In general, it can be concluded that the granular ceramic adsorbent is efficient for the removal of phosphorus in a wide range of pH values.

3.6. Possible mechanism of adsorption

As discussed above, phosphorus adsorption onto granular ceramic adsorbent can be hypothesized to occur via different mechanisms, such as electrostatic attraction, ligand exchange, hydrogen bonding, and chemical precipitation. According to the intra-particle diffusion model, the adsorption process occurs through three stages (Fig. 4): (1) film-diffusion, in which MO on the adsorbent is hydrolyzed to MOH resulting in electrostatic attraction to phosphate species by the protonated surface active sites, while ligand exchange occurs between the complexes and phosphate leading to phosphate transferring from aqueous solution to the adsorbent. Furthermore, if the water environment tend to be basic, chemical precipitation also could occur on the adsorbent surface or in aqueous solutions; (2) inter-particle diffusion, in which the phosphate ions can reach the interior of the material through the aperture and then combine with the active sites present inside of adsorbent; and (3) dynamic equilibrium and precipitation of the distinct thick layer of white phosphate crystal attached on the surface of the treated granular sorbent.

3.7. Desorption and residual metal ions test

Desorption studies were carried out using 10 g L^{-1} phosphorus-adsorbed Hangjin clay granular ceramic
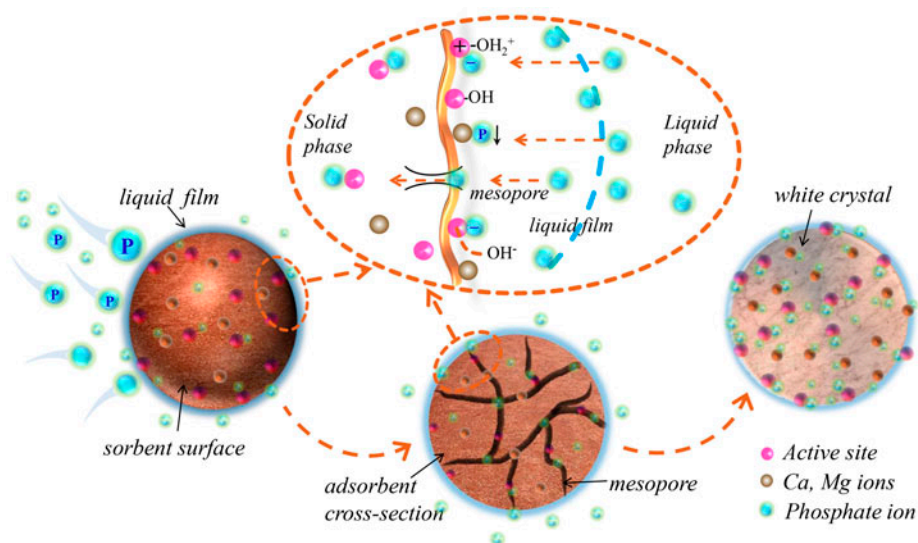
Fig. 4. Schematic illustration of granular ceramic adsorbent and its phosphates sequestration.

Table 6
Concentrations of major inorganic cations in ultrapure water after 24 h

Metal inorganic	K	Ca	Na	Mg	Al	Fe
Concentration (mg L^{-1})	15.8	23.1	8.20	0.31	0.161	0.001

adsorbent at various pH values by adding 0.1 M HCl or NaOH. It was found that the amount of the desorbed phosphorus increased with decreasing pH. When the pH was 2.0, more than 83.53% of adsorbed phosphorus was released into the solution. However, desorption of only 5.82% was obtained when the pH was 7.0, and then slight increased with increasing pH. When the pH reached 13.0, just 20.88% of desorption was observed. The results of these desorption studies may indicate that phosphorus adsorption on the Hangjin clay ceramic adsorbent is not completely reversible. The phosphorus adsorbed by electrostatic attraction and ligand exchange could be desorbed, while the phosphorus adsorbed by chemical precipitation could not be desorbed completely.

A metal dissolution experiment was carried out to study the impact of adsorbent on water quality. The concentrations of the main inorganic cations in treated aqueous solutions are shown in Table 6. The result shows that the metal ions do not exceed the limits set by the drinking water quality standards, although they are detected in ultrapure water. It can be concluded that the composite material did not generally have a significant negative effect on water quality.

4. Conclusions

The present study investigated the effectiveness of an innovative granular ceramic adsorbent based on Hangjin clay in the removal of phosphorus from aqueous solutions. Several advantages of the granular ceramic make the adsorbent a highly effective medium for removing phosphorus at normal pH, including (a) its granular structure, (b) its high surface area, and (c) the low cost of the preparation process from industrial tailings waste. The maximum adsorption capacity of ceramic adsorbent for phosphorus removal was 5.96 mg g^{-1}. The adsorption process followed both the pseudo-second-order and intra-particle diffusion kinetic models, as assesses by the correlation coefficient and chi-square values. Further, the isotherm models suggested that the temperature could affect the adsorption form. The thermodynamic investigation showed that the removal process was spontaneous and endothermic in nature. The adsorption efficiency was found to be independent of the solution pH,

while the concentrations of inorganic cations present in aqueous solutions did not exceed the standard threshold limits for drinking water quality. Electrostatic attraction, ligand exchange, and surface chemical precipitation can be the main mechanism for controlling phosphorus sorption rate. Based on the outcomes of this study, it can be concluded that the use of the granular ceramic adsorbent in practical applications is feasible in addition to facilitating the recycling of the tailings waste, reusing phosphorus, and developing a low cost, but efficient adsorbent.

References

[1] N. Gilbert, Environment: The disappearing nutrient, Nature 461 (2009) 716–718.
[2] D.J. Conley, H.W. Paerl, R.W. Howarth, D.F. Boesch, S.P. Seitzinger, K.E. Havens, C. Lancelot, G.E. Likens, Ecology: Controlling eutrophication: Nitrogen and phosphorus, Science 323 (2009) 1014–1015.
[3] J.A. Camargo, Á. Alonso, M. Puente, Eutrophication downstream from small reservoirs in mountain rivers of Central Spain, Water Res. 39 (2005) 3376–3384.
[4] C. Blöcher, C. Niewersch, T. Melin, Phosphorus recovery from sewage sludge with a hybrid process of low pressure wet oxidation and nanofiltration, Water Res. 46 (2012) 2009–2019.
[5] T. Clark, T. Stephenson, P.A. Pearce, Phosphorus removal by chemical precipitation in a biological aerated filter, Water Res. 31 (1997) 2557–2563.
[6] A. Oehmen, P.C. Lemos, G. Carvalho, Z. Yuan, J. Keller, L.L. Blackall, M.A. Reis, Advances in enhanced biological phosphorus removal: From micro to macro scale, Water Res. 41 (2007) 2271–2300.
[7] L.E. de-Bashan, Y. Bashan, Recent advances in removing phosphorus from wastewater and its future use as fertilizer (1997–2003), Water Res., 38 (2004) 4222–4246.
[8] T. Nur, M.A.H. Johir, P. Loganathan, S. Vigneswaran, J. Kandasamy, Effectiveness of purolite A500PS and A520E ion exchange resins on the removal of nitrate and phosphate from synthetic water, Desalin. Water Treat. 47 (2012) 50–58.

[9] L.M. Blaney, S. Cinar, A.K. Sengupta, Hybrid anion exchanger for trace phosphate removal from water and wastewater, Water Res. 41 (2007) 1603–1613.

[10] Z. Geng, E.R. Hall, P.R. Berube, Membrane fouling mechanisms of a membrane enhanced biological phosphorus removal process, J. Membr. Sci. 296 (2007) 93–101.

[11] P. Loganathan, S. Vigneswaran, J. Kandasamy, N.S. Bolan, Removal and recovery of phosphate from water using sorption, Crit. Rev. Environ. Sci. Technol. 44 (2014) 847–907.

[12] Y. Arai, D.L. Sparks, ATR–FTIR spectroscopic investigation on phosphate adsorption mechanisms at the ferrihydrite–water interface, J. Colloid Interface Sci. 241 (2001) 317–326.

[13] W.T. Chen, C.W. Lin, P.K. Shih, W.L. Chang, Adsorption of phosphate into waste oyster shell: Thermodynamic parameters and reaction kinetics, Desalin. Water Treat. 47 (2012) 86–95.

[14] L. Zhang, L. Wan, N. Chang, J. Liu, C. Duan, Q. Zhou, X. Li, X. Wang, Removal of phosphate from water by activated carbon fiber loaded with lanthanum oxide, J. Hazard. Mater. 190 (2011) 848–855.

[15] Z.L. Shi, F.M. Liu, S.H. Yao, Adsorptive removal of phosphate from aqueous solutions using activated carbon loaded with Fe(III) oxide, New Carbon Mater. 26 (2011) 299–306.

[16] C. Barca, C. Gérente, D. Meyer, F. Chazarenc, Y. Andrès, Phosphate removal from synthetic and real wastewater using steel slags produced in Europe, Water Res. 46 (2012) 2376–2384.

[17] E. Oguz, Removal of phosphate from aqueous solution with blast furnace slag, J. Hazard. Mater. 114 (2004) 131–137.

[18] S. Karaca, A. Gurses, M. Ejder, M. Acikyildiz, Adsorptive removal of phosphate from aqueous solutions using raw and calcinated dolomite, J. Hazard. Mater. 128 (2006) 273–279.

[19] K.S.W. Sing, D.H. Everett, R.A.W. Haul, L. Moscou, R.A. Pierotti, J. Rouquerol, T. Siemieniewska, Reporting physisorption data for gas solid systems with special reference to the determination of surface-area and porosity, Pure Appl. Chem. 57 (1985) 603–619.

[20] G. Leofanti, M. Padovan, G. Tozzola, B. Venturelli, Surface area and pore texture of catalysts, Catal. Today 41 (1998) 207–219.

[21] P.J. Larkin, Infrared and Raman Spectroscopy: Principles and Spectral Interpretation, Elsevier, USA, 2011.

[22] S. Yang, Y. Zhao, R. Chen, C. Feng, Z. Zhang, Z. Lei, Y. Yang, A novel tablet porous material developed as adsorbent for phosphate removal and recycling, J. Colloid Interface Sci. 396 (2013) 197–204.

[23] E. Bulut, M. Özacar, İ.A. Şengil, Equilibrium and kinetic data and process design for adsorption of Congo Red onto bentonite, J. Hazard. Mater. 154 (2008) 613–622.

[24] P.R. Rout, P. Bhunia, R.R. Dash, Modeling isotherms, kinetics and understanding the mechanism of phosphate adsorption onto a solid waste: Ground burnt patties, J. Environ. Chem. Eng. 2 (2014) 1331–1342.

[25] L.A. Rodrigues, M.L.C.P. da Silva, Thermodynamic and kinetic investigations of phosphate adsorption onto hydrous niobium oxide prepared by homogeneous solution method, Desalination 263 (2010) 29–35.

[26] F. Gan, J. Zhou, H. Wang, C. Du, X. Chen, Removal of phosphate from aqueous solution by thermally treated natural palygorskite, Water Res. 43 (2009) 2907–2915.

[27] A.B. Albadarin, A.A.H. Al-Muhtaseb, G.M. Walker, S.J. Allen, M.N.M. Ahmad, Retention of toxic chromium from aqueous phase by H_3PO_4-activated lignin: Effect of salts and desorption studies, Desalination 274 (2011) 64–73.

[28] J.C. Vaghetti, E.C. Lima, B. Royer, B.M. da Cunha, N.F. Cardoso, J.L. Brasil, S.L. Dias, Pecan nutshell as biosorbent to remove Cu(II), Mn(II) and Pb(II) from aqueous solutions, J. Hazard. Mater. 162 (2009) 270–280.

[29] A.B. Albadarin, A.A.H. Al-Muhtaseb, G.M. Walker, S.J. Allen, M.N.M. Ahmad, Retention of toxic chromium from aqueous phase by H_3PO_4-activated lignin: Effect of salts and desorption studies, Desalination 274 (2011) 64–73.

[30] A. Naeem, P. Westerhoff, S. Mustafa, Vanadium removal by metal (hydr)oxide adsorbents, Water Res. 41 (2007) 1596–1602.

[31] Y. Zeng, H. Woo, G. Lee, J. Park, Adsorption of Cr(VI) on hexadecylpyridinium bromide (HDPB) modified natural zeolites, Microporous Mesoporous Mater. 130 (2010) 83–91.

[32] R. Sips, On the structure of a catalyst surface, J. Chem. Phys. 16 (1948) 490–495.

[33] O. Redlich, D.L. Peterson, A useful adsorption isotherm, J. Phys. Chem. 63 (1959) 1024–1027.

[34] K.N. Chen, K.Q. Zhao, H.H. Zhang, Q.F. Sun, Z.L. Wu, Y.M. Zhou, Y.C. Zhong, F. Ke, Phosphorus removal from aqueous solutions using a synthesized adsorbent prepared from mineralized refuse and sewage sludge, Environ. Technol. 34 (2013) 1489–1496.

[35] W. Wang, H. Zhang, L. Zhang, H. Wan, S. Zheng, Z. Xu, Adsorptive removal of phosphate by magnetic Fe_3O_4@C@ZrO_2, Colloids Surf., A: Physicochem. Eng. Aspects 469 (2015) 100–106.

[36] B.M. Spears, S. Meis, A. Anderson, M. Kellou, Comparison of phosphorus (P) removal properties of materials proposed for the control of sediment p release in UK lakes, Sci. Total Environ. 442 (2013) 103–110.

[37] K.A. Krishnan, A. Haridas, Removal of phosphate from aqueous solutions and sewage using natural and surface modified coir pith, J. Hazard. Mater. 152 (2008) 527–535.

[38] M.A. Wahab, R.B. Hassine, S. Jellali, *Posidonia oceanica* (L.) fibers as a potential low-cost adsorbent for the removal and recovery of orthophosphate, J. Hazard. Mater. 191 (2011) 333–341.

[39] C. Namasivayam, D. Sangeetha, Equilibrium and kinetic studies of adsorption of phosphate onto $ZnCl_2$ activated coir pith carbon, J. Colloid Interface Sci. 280 (2004) 359–365.

[40] L.G. Yan, Y.Y. Xu, H.Q. Yu, X.D. Xin, Q. Wei, B. Du, Adsorption of phosphate from aqueous solution by hydroxy-aluminum, hydroxy-iron and hydroxy-iron-aluminum pillared bentonites, J. Hazard. Mater. 179 (2010) 244–250.

[41] N. Pitakteeratham, A. Hafuka, H. Satoh, Y. Watanabe, High efficiency removal of phosphate from water by zirconium sulfate-surfactant micelle mesostructure immobilized on polymer matrix, Water Res. 47 (2013) 3583–3590.

[42] H.B. Bradl, Adsorption of heavy metal ions on soils and soils constituents, J. Colloid Interface Sci. 277 (2004) 1–18.

[43] D.M. Sherman, S.R. Randall, Surface complexation of arsenic(V) to iron(III) (hydr)oxides: Structural mechanism from *ab initio* molecular geometries and EXAFS spectroscopy, Geochim. Cosmochim. Acta 67 (2003) 4223–4230.

[44] E. Sabah, M. Majdan, Removal of phosphorus from vegetable oil by acid-activated sepiolite, J. Food Eng. 91 (2009) 423–427.